Enhanced radiative recombination rate for electron-hole droplets in a silicon photonic crystal nanocavity

Toshiyuki Ihara,[1,*] Yasushi Takahashi,[2] Susumu Noda,[3,4] and Yoshihiko Kanemitsu[1,4]
[1]*Institute for Chemical Research, Kyoto University, Uji, Kyoto 611-0011, Japan*
[2]*Department of Physics and Electronics, Osaka Prefecture University, Gakuen-cho, Naka-ku, Sakai, Osaka 599-8570, Japan*
[3]*Department of Electronic Science and Engineering, Kyoto University, Katsura, Nishikyo-Ku, Kyoto 615-8510, Japan*
[4]*Photonics and Electronics Science and Engineering Center, Kyoto University, Kyoto 615-8510, Japan*
(Received 25 October 2016; revised manuscript received 21 April 2017; published 10 July 2017)

We investigate photoluminescence (PL) spectra and dynamics of clean silicon photonic crystal nanocavities at 10 K. A sharp emission peak due to the nanocavity mode has the largest intensity when the energy of the nanocavity mode is equal to the emission energy of the electron-hole droplets (EHDs). Time-resolved PL spectroscopy indicates that the PL lifetime of the EHD is reduced to as short as 1.2 ns by the nanocavity mode. A careful analysis of the lifetimes indicates that the radiative recombination rate for EHD is enhanced by a factor of larger than 5 by the Purcell effect.

DOI: 10.1103/PhysRevB.96.035303

I. INTRODUCTION

The development of high-efficiency silicon (Si) light emitters is a long-standing issue and is attracting a lot of attention owing to the potential for fabricating inexpensive, monolithic optoelectronic chips with complementary metal-oxide-semiconductor (CMOS) compatibility [1–7]. Si, however, has an indirect energy band gap, with a very low efficiency of radiative electron-hole recombination. Because the quantum efficiency (η) of the radiative process is determined by the relative magnitudes of the radiative recombination rate (k_R) and the nonradiative recombination rate (k_{NR}), a key to enhance η is to increase the k_R and decrease the k_{NR}. To realize these requirements, several Si engineered materials have been studied where nanostructured Si systems such as nanocrystals [8–10], nanolayers [11–13], nanowires [14–16], and heterostructures with SiO_2 and Ge [17–21] have shown promising properties. However, there is still no faultless solution for achieving practical Si emitters.

For Si at room temperature, k_{NR} is generally much larger than k_R, and the thermal energy is greater than the exciton-binding energy (14.3 meV [22]). Thus, only a broad, low-intensity emission peak originating from the electron-hole plasma (EHP) is observed at room temperature when we pump the Si with high excitation power. However, optically pumped Si at a low temperature shows various sharp peaks reflecting the electron-hole many-body interactions [23,24]. It is well known that a strong optical excitation of Si below 30 K results in the formation of a unique condensation state known as an electron-hole droplet (EHD) [25–28]. This is a peculiar electron-hole phase of indirect-band-gap semiconductors, which cannot be observed in direct-gap III-V compound semiconductors [23–31]. Because the emission peak for the EHD can be larger than those for free exciton (FE) and EHP, studies for enhancing the EHD emission using nanostructured Si have attracted much attention [15,32,33]. However, nanostructured materials tend to increase the surface recombination processes of carriers, and electron holes in EHD will increase the Auger processes owing to the high carrier density [34]. These phenomena increase the k_{NR} and, thus a large increase in EHD emission, as the situation where k_R is greater than k_{NR} is difficult to achieve. A unique mechanism for increasing k_R is desirable for further enhancement.

Two-dimensional photonic crystal (PC) nanocavities have high-quality factors (Q) and small modal volumes (V) of almost one cubic wavelength in the material [35–38]. Their high Q/V values are beneficial for the study of the Purcell effect, which enhances the spontaneous emission rate of the material [39,40]. There are many reports of enhanced k_R due to the Purcell effect for the emission of FE or EHP in nanocavities consisting of III-V compound semiconductors [41–43]. However, an enhanced k_R due to the Purcell effect has not been demonstrated in Si nanocavities, although enhanced emission peaks suggesting the Purcell effect have been reported [44–47]. Si nanocavities have achieved the highest Q values for PC cavities because of well-developed nanofabrication techniques and the high purity of the substrates [38]. Therefore, the developments of novel emitters are expected for Si nanocavities [48]. From this background, it is very interesting to investigate the Purcell effect for EHD emission in Si nanocavities.

Here, we report on time-resolved PL (TRPL) spectroscopy for clean Si nanocavities at 10 K. The resonant mode energies of the nanocavities are accurately controlled to overlap with the emission energies of FE, EHP, and EHD. In all the samples, we observed sharp emission peaks in the nanocavity mode with a Q factor of 1500. These peaks were enhanced when the energy of the nanocavity mode overlapped the energy of the EHD emission. A careful analysis using TRPL spectra reveals that the PL lifetime of the EHD is reduced to as short as 1.2 ns in the nanocavity mode. A comparison of the lifetimes for three measurement positions, PC area with a nanocavity, PC area without a nanocavity, and substrate area without a PC, indicates that the k_R for EHD is enhanced by a factor of larger than 5 by the Purcell effect.

*Present address: Advanced ICT Research Institute, National Institute of Information and Communications Technology, Kobe 651-2492, Japan.

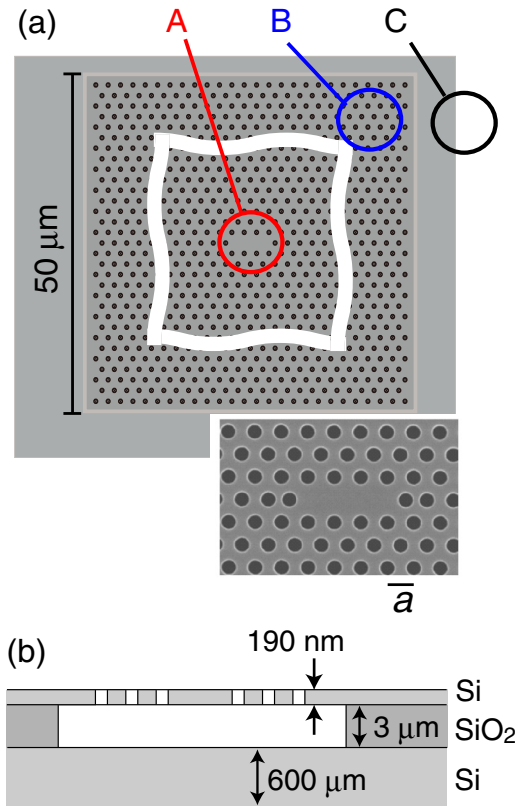

FIG. 1. (a) Schematic of a measured sample, with an L3 nanocavity located at the center. The positions A–C indicate the excitation points that were used for obtaining the spectra. (b) Cross-sectional sketch of a Si slab with an air-suspended structure.

II. SAMPLE STRUCTURE AND EXPERIMENTAL SETUP

Figure 1(a) shows a schematic of a measured sample. The PC consists of a triangular lattice of circular air holes with radii of 90 nm, and the pattern is formed in a square area of $50 \times 50\,\mu$m. An L3 nanocavity, consisting of three missing air holes, with neighboring air holes shifted to the outside of the cavity by 0.15 lattice constants (a) is embedded at the center [36]. The inset shows a scanning electron microscope (SEM) image of a nanocavity. We utilized a Si-on-insulator (SOI) substrate with a Si slab thickness of 190 nm and a resistivity greater than 13.5 Ω cm(p type, boron doping). The 3000-nm-thick SiO_2 layer underneath the patterned region was selectively removed by hydrofluoric acid to form an air-bridge structure, as shown in Fig. 1(b). The fabrication process was the same as that for a previous report which reports nanocavities with Q factors greater than several million [49]. We have so far increased the Q factors of Si nanocavities by reducing the absorption loss [38,50,51]. Thus, the measured samples can have a surface with very few contaminations, a low level of impurities, and reduced surface defect states (the surface might be slightly oxidized since the samples were kept in a standard desiccator with a relative humidity of 30% for several months). Clean nanocavities result in a decrease of the k_{NR}, which is significant to detect enhanced k_R due to the Purcell effect. In order to resonate the wavelength of the nanocavity mode to the energies of the Si emission peaks, we fabricated several tens of samples on the same chip with different a ranging from 312 to 350 nm in increments of 1 nm.

We used a diode laser operating at a wavelength of 405 nm as an excitation source for both time-integrated PL and TRPL measurements. The excitation pulse for the TRPL measurement had a duration of 50 ps at a repetition frequency of 1 MHz. The time-integrated PL measurements were performed with continuous-wave excitation. The use of a short wavelength can decrease the excitation light reaching the substrate because of the strong absorption by the top Si layer ($\alpha \cong 10^5\,\mathrm{cm}^{-1}$ at 405 nm [52]). An objective lens with a numerical aperture of 0.42 in the near-infrared region was used to excite the sample with a spot size of a few μm. The same lens was used to collect the PL signal from the sample. The polarizer was not used in the measurement. Time-integrated PL spectra were measured using an InGaAs detector mounted on a spectrometer with a focal length of 30 cm and a resolution of 2 meV. To obtain the temporal line shape of the TRPL spectra, we used a streak camera for the near-infrared region (Hamamatsu Photonics) equipped with a spectrometer of 15 cm focal length. The resolution of the detection system was set to be high enough (3 meV) to detect the energy differences between FE, EHP, and EHD. To obtain TRPL data with a sufficient signal-to-noise ratio, the signal was integrated for 30 min. We performed the measurements for the three positions denoted in Fig. 1(a): position A with the nanocavity, position B with only PC patterns, and position C without the PC patterns. The samples were maintained at 10 K in a cryostat. All TRPL measurements for positions A–C were performed within a day to ensure the same surface conditions.

III. EXPERIMENTAL RESULTS

A. Time-integrated PL spectroscopy

Figure 2(a) shows PL spectra for cw excitation measured at position A for three samples with $a = 348$ (bottom), 340 (middle), and 332 nm (top). For $a = 348$ nm, a sharp peak was observed at 1.060 eV, which originates from the fifth resonant mode in the nanocavity [44]. The peak at 1.100 eV originates from FE coupled with transverse-optical (TO) phonons [53]. The broad peak at 1.085 eV should be attributed to electron-hole condensations of the EHP or EHD because their energies are typically in this range [25,26,33]. For $a = 340$ nm, the peak due to the fifth mode appears at 1.085 eV with increased intensity compared to that for the sample with $a = 348$ nm. Other PL peaks at 1.020, 1.027, and 1.118 eV are attributed to the third and fourth resonant modes, and the band edge modes, respectively [44]. At $a = 332$ nm, the fifth mode appears at 1.110 eV. Figure 2(b) shows the change in photon energies of the cavity modes for samples with lattice constants ranging from 312 to 350 nm. The energies of the cavity modes increase with decreasing lattice constants, while the FE peak at 1.100 eV and a broad peak at 1.085 eV are unchanged. The peak energy of the fifth mode overlaps with the emission energies of electron-hole condensations and FE. The fifth mode is isolated from the other modes and it has a large collection efficiency through the objective lens [44,45]. Therefore, the fifth mode is appropriate for the TRPL measurement to investigate the Purcell

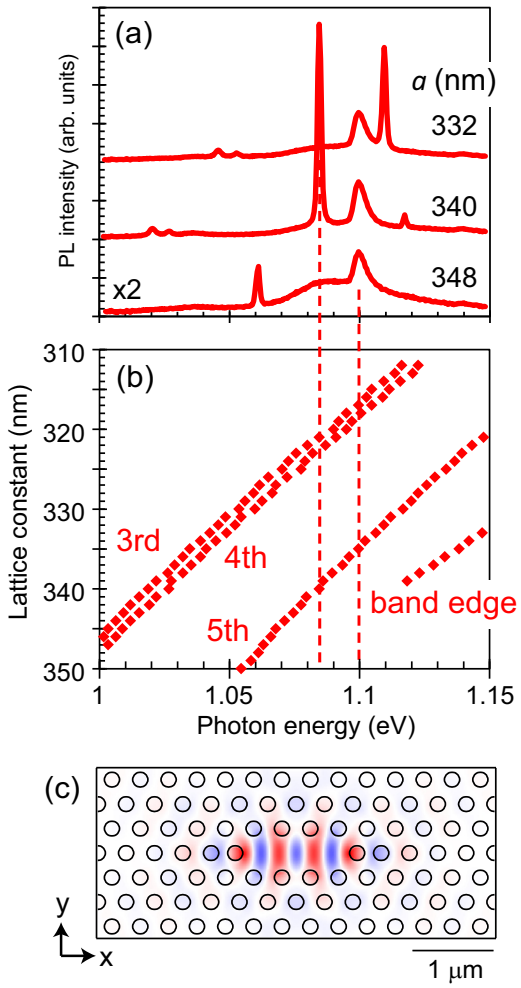

FIG. 2. (a) Time-integrated PL spectra obtained from samples with lattice constants of 332, 340, and 348 nm. (b) Peak photon energy of cavity modes measured for samples with lattice constants from 320 to 350 nm with an increment of 1 nm. (c) An image of the electric field of the fifth cavity mode of a sample with $a = 339$ nm calculated by the FDTD method.

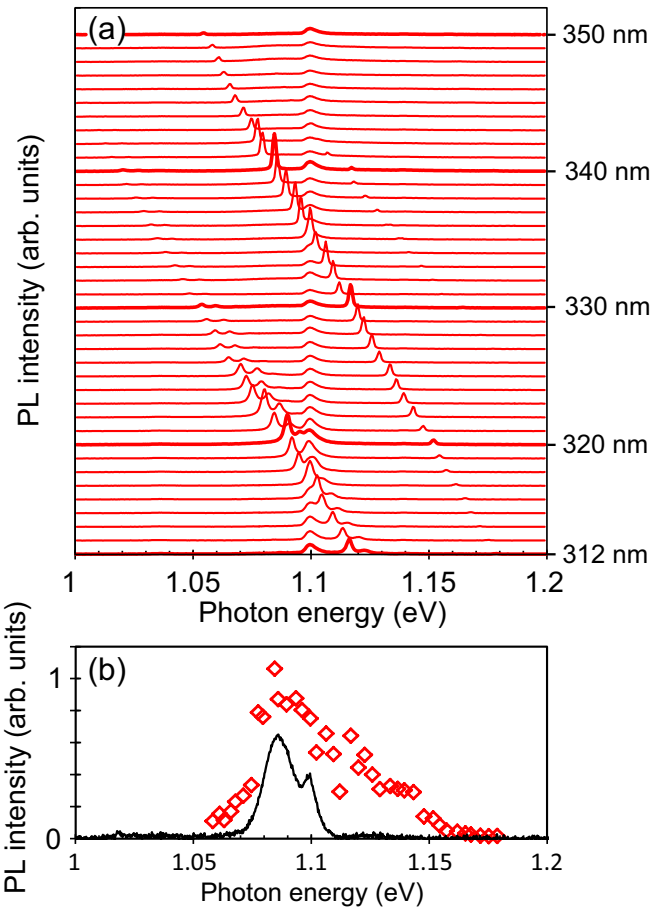

FIG. 3. (a) Spectra for the samples with $a = 312-350$ nm. (b) Plot for the integrated intensity of the fifth mode peak as a function of the peak energy. The black line is a PL spectrum measured at position C.

effect. Figure 2(c) shows the electric field distributions E_y calculated by the finite difference time domain (FDTD) method. The calculated Q value is ~1500, which should be sufficient for investigating the Purcell effect in Si because the Q factor for the intrinsic linewidth of Si emission is smaller [46,54].

Figure 3(a) presents the entire spectra for all the samples with $a = 312-350$ nm. The symbols in Fig. 3(b) show the integrated intensity of the fifth mode peak as a function of the peak energy where the contributions of the original intensities of the FE peak and broad emission peak are subtracted. The emission peak is most enhanced at ~1.085 eV, corresponding to the energy for the electron-hole condensations, not at the FE energy of 1.100 eV. Furthermore, Fig. 3(b) indicates that the emission is also enhanced at 1.12 eV, which would be the energy for condensation states coupled to transverse-acoustic (TA) phonons [33]. The solid curve in Fig. 3(b) shows a PL spectrum measured at position C. The main peaks at 1.085 and 1.10 eV are the EHD emission and the FE emission for TO phonons, respectively. The contribution of EHD emission for TA phonons is also observed at 1.125 eV, though it is very small. The intensity of the nanocavity emission becomes strongest between 1.08 and 1.09 eV, which agrees with the emission peak of the EHD emission for TO phonons. Thus, these spectra indicate that the emission enhancement by the nanocavity mode is important for the condensation states, especially for EHD emission. These features are quite different from those in the previous report, which indicated the emission enhancement of FE and the surface defect band [47]. We consider that these contrastive results originate from the sample quality or experimental conditions in temperature and excitation power. In the rest of the paper, we focus on the enhanced emission from the condensation states coupled with TO phonons.

B. Time-resolved PL spectroscopy

Figures 4(a) and 4(b) show TRPL images of the sample with $a = 339$ nm measured at positions A and B, respectively. The excitation power of the pulsed light is 30 μW on the surface, which is enough power to create the EHD. The PL intensities are plotted in a color scale as functions of time and photon energy. We observed clear signals for both positions around 1.080–1.100 eV in the time range from 0 to 4 ns. The

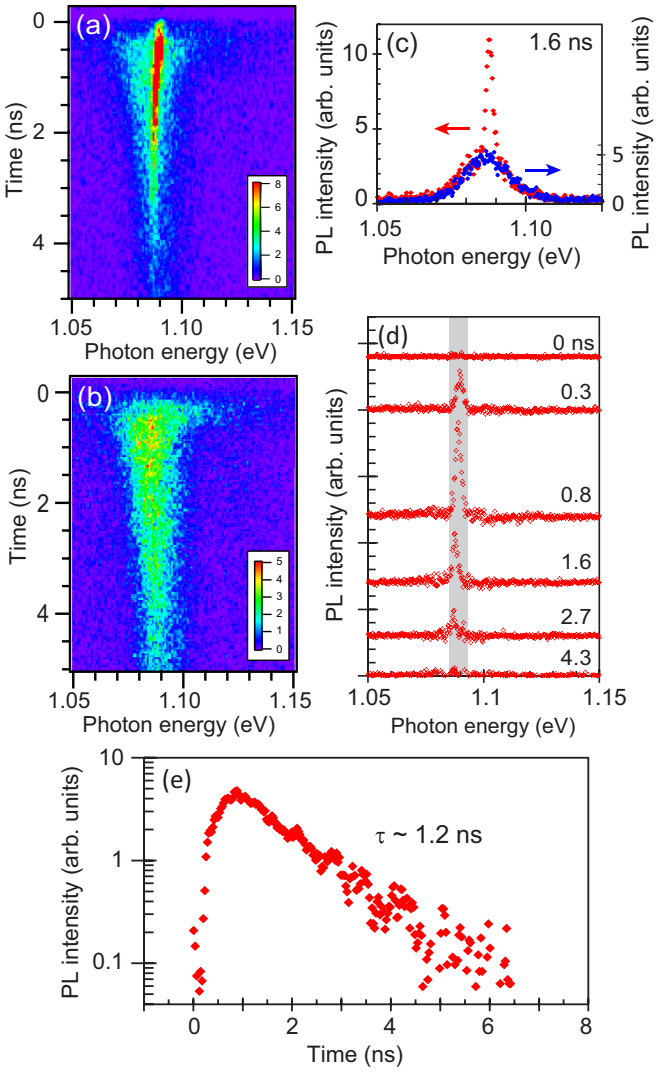

FIG. 4. (a) A TRPL image measured on a PC with $a = 339$ nm at position A. (b) A TRPL image measured on a PC with $a = 339$ nm at position B. (c) Temporal PL spectra for position A (red) and position B (blue) at 1.6 ns obtained from the data in (a) and (b). (d) Temporal PL spectra for the cavity mode from 0 to 4.3 ns. (e) Decay profile for position A obtained by integrating from 1.085 to 1.093 eV.

red dots in Fig. 4(c) show a temporal PL spectrum at 1.6 ns obtained from Fig. 4(a). A strong, sharp peak at 1.088 eV with a full width at half maximum (FWHM) of 3 meV, and a broad background signal with FWHM of 20 meV are observed. The FE peak at 1.100 eV is not seen in the initial time range since the carrier density is too high to form an exciton. We add a temporal PL spectrum obtained from Fig. 4(b) at 1.6 ns as blue dots with the right axis where only the broad peak was observed. It is noted that the PL line shape at position B is almost the same for the background signal observed at position A, though the intensity at position A is 0.6 times smaller. Thus, we assigned the sharp and broad background signals for position A to emission from the fifth nanocavity mode and to that from PC structures surrounding the cavity, respectively.

In order to derive the lifetime for the nanocavity mode emission, we have to distinguish the nanocavity mode signal

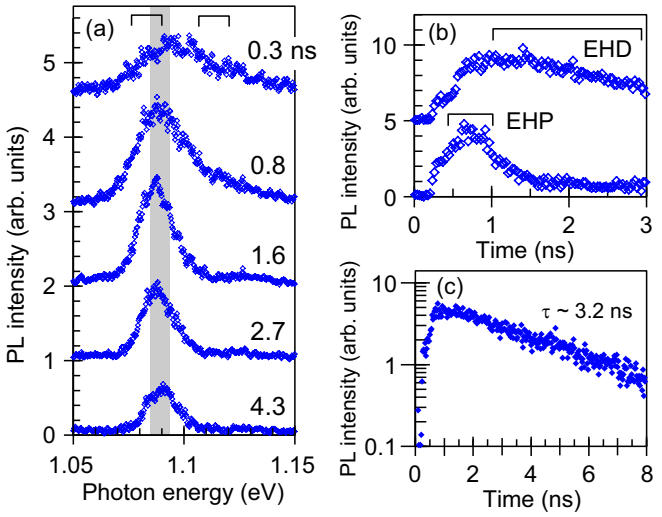

FIG. 5. (a) Temporal PL spectra at position B from 0.3 to 4.3 ns. (b) Decay profiles obtained by integrating from 1.076 to 1.091 eV (top) and from 1.105 to 1.120 eV (bottom). (c) A decay profile with a larger scale for data integration from 1.085 to 1.093 eV.

from the background signal. Figure 4(d) shows temporal PL spectra at various times from 0 to 4.3 ns, obtained from the data at position A [Fig. 4(a)] after subtracting 60% of the data at position B [Fig. 4(b)]. A flat offset level and a sharp cavity mode signal were observed for all the spectra, which proves the validity of this analytical method. The cavity mode gradually increases its intensity from 0 to 0.8 ns, loses its intensity after 0.8 ns, and almost disappears at 4.3 ns. The FWHM, which is determined by the resolution limit of the spectrometer, was ~3 meV for all signals. The cavity mode peak appears at 1.090 eV at 0.3 ns, while it appears at 1.087 eV at 2.7 ns. The shift of 3 meV is probably due to the reduction of refractive index (~0.27%) caused by optically induced carriers [55,56]. Figure 4(e) shows the decay dynamics of the cavity mode signal, which is produced by integrating the spectra in Fig. 4(d) from 1.085 to 1.093 eV; the integration window is shown in gray. Figure 4(e) shows a single exponential decay with a lifetime of 1.2 ns, which is very short. We would now like to determine whether the short lifetime is caused by the Purcell effect or by increased k_{NR}. We will also attempt to identify whether the carrier state for the nanocavity mode emission is EHD or EHP.

Next, we analyze the results at position B: Figure 5(a) shows the temporal PL spectra at various times from 0 to 4.3 ns, obtained from Fig. 4(b). At 0.3 ns, the broad emission has a peak energy of 1.100 eV and a FWHM of 40 meV. Although the peak energy is the same as that for the FE peak shown in Fig. 2(a), the emission should not be attributed to FE because of the larger FWHM. At 0.8 ns, the peak width narrows to 30 meV and the peak energy shifts to 1.090 eV with a slightly increased intensity. At 1.6 ns, the peak appears at 1.085 eV with a FWHM of 20 meV. After 1.6 ns, the peak intensity decreases without any change in the line shape or the energy.

Figure 5(b) shows the initial decay dynamics integrated for the energy regions for 1.076–1.091 eV (top) and for 1.105–1.120 eV (bottom), respectively. The square brackets in Fig. 5(a) indicate these energy regions. The bottom plot for the

higher energy region shows a rapid increase and fast drop for 0–1.6 ns while the top plot for the lower energy region shows a delayed rise time of about 0.8 ns and a slow decrease. This difference between the lower and higher energy sides of the broad peak indicates the transformation of the electron-hole system from EHP to EHD [25,28]. The narrowing phenomenon and the peak shift observed in Fig. 5(a) also indicate the transformation process to EHD. Therefore, we can roughly classify the origin of the broad emission as follows: The broader peak observed before 1.0 ns corresponds to EHP emission while the peak after 1.0 ns originates from the EHD. The rise time of the nanocavity mode presented in Fig. 4(e) is also 0.8 ns, and the time evolution of the broad background signal for position A is the same as that for position B, as explained in Fig. 4(d). Figure 3(b) and these experimental features indicate that the main source of the nanocavity mode emission should be attributed to EHD. The EHP before the transformation to the EHD could partly contribute to the emission.

Figure 5(c) shows the decay plot at position B obtained from the integration at 1.085–1.093 eV, which is the same condition that was used for position A [Fig. 4(e)]. The data show a single exponential decay with a lifetime of 3.2 ns, which is longer than the lifetime for the nanocavity mode of 1.2 ns in Fig. 4(e). The decreased lifetime at position A is not due to the increase of nonradiative surface recombination, since the number of air holes at position A is smaller than at position B. The increase of the relaxation for momentum conservation law close to the surface is also rejected for the same reason. The transformation process from the EHP to EHD is also not the origin, since it is almost completed in the initial phase before 1.0 ns. Stimulated emission also will not be a suitable explanation because the Q factor of the nanocavity mode used in the experiment is not so high that the number of photons stored in the cavity is larger than one [41,43] Therefore, we conclude that the shortened lifetime in Fig. 4(e) should be attributed to the Purcell effect.

Finally, we compare the above results with the decay curve obtained at position C in order to estimate the Purcell factor. Figure 6(a) shows a TRPL image measured at position C, where no photonic pattern is fabricated. A broad PL signal appeared between 1.080 and 1.100 eV. Figure 6(b) shows the temporal PL spectra. The spectral evolution agrees with that for position B presented in Fig. 5(a). Therefore, the main source of the emission at position C is also EHD after 1.0 ns. Figure 6(c) shows a decay curve obtained from the integration at 1.085–1.093 eV where a rise time of about 0.8 ns as in Figs. 4(e) and 5(c) is observed. By using single exponential fitting, the PL decay lifetime was estimated to be 10 ns. The increase of the lifetime from that at position B can be explained by a decrease of surface recombination processes caused by the absence of an air-hole structure.

IV. DISCUSSION

Here, we use the relation for the PL recombination rate $k = k_R + k_{NR}$ to estimate the Purcell factor for EHD emission. We define the rates for the three positions as follows,

$$k^A = k_R^A + k_{NR}^A, \quad k^B = k_R^B + k_{NR}^B,$$
$$k^C = k_R^C + k_{NR}^C = k_R^C\left(1 + \frac{k_{NR}^C}{k_R^C}\right). \tag{1}$$

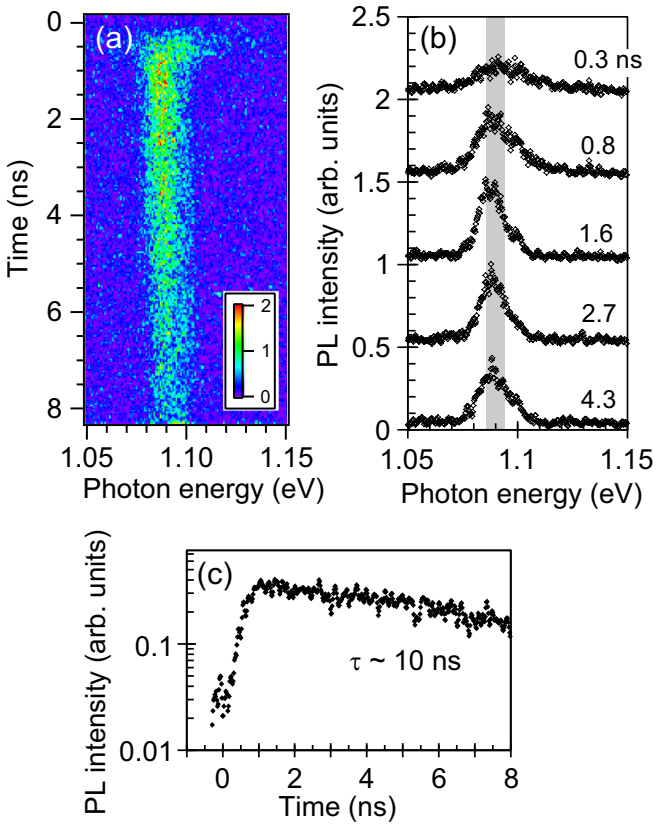

FIG. 6. (a) A TRPL image measured at position C. (b) Temporal PL spectra from 0.3 to 4.3 ns. (c) A decay profile obtained by integrating from 1.085 to 1.093 eV.

The lifetime of 1.2 ns at position A corresponds to the rate of $k^A = (1/1.2) \times 10^9$. Similarly, $k^B = (1/3.2) \times 10^9$ and $k^C = (1/10) \times 10^9$. We assume $k_{NR}^A = k_{NR}^B$. Then, the following relation is derived,

$$\frac{k^A - k^B}{k^C} = \left(\frac{k_R^A}{k_R^C} - \frac{k_R^B}{k_R^C}\right)\left(1 + \frac{k_{NR}^C}{k_R^C}\right)^{-1}. \tag{2}$$

The Purcell factor F_p is expressed as follows,

$$F_p \equiv \frac{k_R^A}{k_R^C} = \frac{k^A - k^B}{k^C}\left(1 + \frac{k_{NR}^C}{k_R^C}\right) + \frac{k_R^B}{k_R^C} \geqslant \frac{k^A - k^B}{k^C}. \tag{3}$$

Then, the Purcell factor is estimated to be larger than at least 5.2 from $(k^A - k^B)/k^C = 5.2$. When we assume $k_{NR}^A = k^B = (1/3.2) \times 10^9$, k_R^A is estimated to be $(1/1.2 - 1/3.2) \times 10^9$. Then, the η for EHD at position A is estimated to be probably larger than 0.6 ($\eta = k_R^A/k^A = 1 - 1.2/3.2$), which means the situation where the k_R is larger than the k_{NR} is achieved. This is surprising because the decrease in the PL lifetimes in nanostructures without surface oxidation has usually been interpreted as an increase in the k_{NR} owing to surface recombination.

It is noticed that the three decay spectra shown in Figs. 4(e), 5(c), and 6(c) are produced by extracting a part of the EHD emission between 1.085 and 1.093 eV. In addition, we subtract the background emission from the emission at position A, deriving the decay plot shown in Fig. 4(e). Therefore, we cannot correctly estimate η of the entire emission for the Si

nanocavity from these results. The situation where k_R is larger than k_{NR} is realized for a part of the photoexcited carrier. The rest of the photoexcited carrier, probably existing outside the cavity mode, appears as the background signal. When we decrease the excitation spot size and the detection area to less than the cavity size, the situation of $k_R \geqslant k_{NR}$ may be observed for the entire emission. However, the experimental results presented in this work strongly suggest a large potential of the Purcell effect in Si nanocavities.

Earlier experiments on similar Si nanocavities at room temperature suggested that the Purcell factor could be from 5 to 10 [44,45]. Another experiment also indicated that a higher temperature stability of the nanocavity mode emission might arise from an enhanced η due to the Purcell effect [47]. Here, we directly demonstrate the enhanced k_R due to the Purcell effect for the condensation state of the EHD. Such a mechanism would be useful for the development of Si emitters. For example, it can be utilized for the pump light source of ultralow-threshold Raman Si lasers using heterostructure high-Q nanocavities [48].

V. CONCLUSIONS

We have demonstrated an enhanced k_R for EHD emission in Si nanocavities owing to the Purcell effect. Experimental results indicate that the Purcell factor can be larger than 5. It should be emphasized that the enhanced k_R due to the nanocavity mode is greater than the increased k_{NR} in our Si nanocavities. These findings will stimulate reconsideration of EHD dynamics in Si crystals and nanostructures and the development of Si light emitters.

ACKNOWLEDGMENTS

The authors thank Dr. M. Yamaguchi for fruitful discussions regarding the Purcell factor. Part of this work was supported by the Collaborative Research Program of the Institute for Chemical Research, Kyoto University (Grants No. 2013-15 and No. 2012-46), KAKENHI (Grant No. 15H05428), CPHoST program, and CREST, Japan Science and Technology Agency (Grant No. JPMJCR16N3).

T.I. and Y.T. contributed equally to this work.

[1] *Light Emission in Silicon: From Physics to Devices*, edited by D. J. Lockwood, Semiconductors and Semimetals Vol. 49 (Academic Press, San Diego, 1997).
[2] L. Pavesi, S. Gaponenko, and L. Dal Negro, *Towards the First Silicon Laser* (Kluwer Academic, Dordrecht, 2003).
[3] S. S. Iyer and Y. H. Xie, Science **260**, 40 (1993).
[4] Y. Kanemitsu, Phys. Rep. **263**, 1 (1995).
[5] A. G. Cullis, L. T. Canham, and P. D. J. Calcott, J. Appl. Phys. **82**, 909 (1997).
[6] M. A. Green, J. Zhao, A. Wang, P. J. Reece, and M. Gal, Nature (London) **412**, 805 (2001).
[7] E. G. Barbagiovanni, D. J. Lockwood, P. J. Simpson, and L. V. Goncharova, Appl. Phys. Rev. **1**, 011302 (2014).
[8] H. Takagi, H. Ogawa, Y. Yamazaki, A. Ishizaki, and T. Nakagiri, Appl. Phys. Lett. **56**, 2379 (1990).
[9] L. T. Canham, Appl. Phys. Lett. **57**, 1046 (1990).
[10] Y. Kanemitsu, T. Ogawa, K. Shiraishi, and K. Takeda, Phys. Rev. B **48**, 4883 (1993).
[11] D. J. Lockwood, Z. H. Lu, and J. M. Baribeau, Phys. Rev. Lett. **76**, 539 (1996).
[12] Y. Kanemitsu and S. Okamoto, Phys. Rev. B **56**, R15561 (1997).
[13] G. F. Grom, D. J. Lockwood, J. P. McCaffrey, H. J. Labbe, P. M. Fauchet, B. White, J. Diener, D. Kovalev, F. Koch, and L. Tsybeskov, Nature (London) **407**, 358 (2000).
[14] Y. Kanemitsu, H. Sato, S. Nihonyanagi, and Y. Hirai, Phys. Status Solidi A **190**, 755 (2002).
[15] O. Demichel, V. Calvo, N. Pauc, A. Besson, P. Noé, F. Oehler, P. Gentile, and N. Magnea, Nano Lett. **9**, 2575 (2009).
[16] J. Valenta, B. Bruhn, and J. Linnros, Nano Lett. **11**, 3003 (2011).
[17] V. S. Bagaev, V. S. Krivobok, S. N. Nikolaev, A. V. Novikov, E. E. Onishchenko, and M. L. Skorikov, Phys. Rev. B **82**, 115313 (2010).
[18] T. M. Burbaev, M. N. Gordeev, D. N. Lobanov, A. V. Novikov, M. M. Rzaev, N. N. Sibeldin, M. L. Skorikov, V. A. Tsvetkov, and D. V. Shepel, JETP Lett. **92**, 305 (2010).
[19] O. Demichel, V. Calvo, P. Noé, B. Salem, P.-F. Fazzini, N. Pauc, F. Oehler, P. Gentile, and N. Magnea, Phys. Rev. B **83**, 245443 (2011).
[20] V. S. Bagaev, V. S. Krivobok, S. N. Nikolaev, E. E. Onishchenko, M. L. Skorikov, A. V. Novikov, and D. N. Lobanov, JETP Lett. **94**, 63 (2011).
[21] Y. Kanemitsu, J. Lumin. **100**, 209 (2002).
[22] K. L. Shaklee and R. E. Nahory, Phys. Rev. Lett. **24**, 942 (1970).
[23] C. F. Klingshirn, *Semiconductor Optics* (Springer, Berlin, 1995).
[24] C. D. Jeffries and L. V. Keldy, *Electron-Hole Droplets in Semiconductors* (North-Holland, Amsterdam, 1983).
[25] J. Shah, M. Combescot, and A. H. Dayem, Phys. Rev. Lett. **38**, 1497 (1977).
[26] L. M. Smith and J. P. Wolfe, Phys. Rev. B **51**, 7521 (1995).
[27] M. Tajima and S. Ibuka, J. Appl. Phys. **84**, 2224 (1998).
[28] T. Suzuki and R. Shimano, Phys. Rev. Lett. **103**, 057401 (2009).
[29] R. Shimano, M. Nagai, K. Horiuch, and M. Kuwata-Gonokami, Phys. Rev. Lett. **88**, 057404 (2002).
[30] D. Bimberg, M. S. Skolnick, and W. J. Choyke, Phys. Rev. Lett. **40**, 56 (1978)
[31] D. Hirano, T. Kimoto, and Y. Kanemitsu, J. Phys. Soc. Jpn. **82**, 063703 (2013).
[32] N. Pauc, V. Calvo, J. Eymery, F. Fournel, and N. Magnea, Phys. Rev. Lett. **92**, 236802 (2004).
[33] S. Nihonyanagi and Y. Kanemitsu, Appl. Phys. Lett. **85**, 5721 (2004).
[34] J. J. Dziewior and W. Schmid, Appl. Phys. Lett. **31**, 346 (1977).
[35] S. Noda, A. Chutinan, and M. Imada, Nature (London) **407**, 608 (2000).
[36] Y. Akahane, T. Asano, B. S. Song, and S. Noda, Nature (London) **425**, 944 (2003).
[37] B. S. Song, S. Noda, T. Asano, and Y. Akahane, Nat. Mater. **4**, 207 (2005).
[38] H. Sekoguchi, Y. Takahashi, T. Asano, and S. Noda, Opt. Express **22**, 916 (2014).

[39] E. M. Purcell, H. C. Torrey, and R. V. Pound, Phys. Rev. **69**, 37 (1946).
[40] S. Noda, M. Fujita, and T. Asano, Nat. Photonics **1**, 449 (2007).
[41] D. Englund, D. Fattal, E. Waks, G. Solomon, B. Zhang, T. Nakaoka, Y. Arakawa, Y. Yamamoto, and J. Vuckovic, Phys. Rev. Lett. **95**, 013904 (2005).
[42] W. H. Chang, W. Y. Chen, H. S. Chang, T. P. Hsieh, J. I. Chyi, and T. M. Hsu, Phys. Rev. Lett. **96**, 117401 (2006).
[43] K. Hennessy, A. Badolato, M. Winger, D. Gerace, M. Atatüre, S. Gulde, S. Falt, E. L. Hu, and A. Imamoglu, Nature (London) **445**, 896 (2007).
[44] S. Iwamoto, Y. Arakawa, and A. Gomyo, Appl. Phys. Lett. **91**, 211104 (2007).
[45] M. Fujita, Y. Tanaka, and S. Noda, IEEE J. Sel. Top. Quantum Electron. **14**, 1090 (2008).
[46] S. Nakayama, S. Ishida, S. Iwamoto, and Y. Arakawa, Appl. Phys. Lett. **98**, 171102 (2011).
[47] N. Hauke, T. Zabel, K. Müller, M. Kaniber, A. Laucht, D. Bougeard, G. Abstreiter, J. J. Finley, and Y. Arakawa, New J. Phys. **12**, 053005 (2012).
[48] Y. Takahashi, Y. Inui, M. Chihara, T. Asano, R. Terawaki, and S. Noda, Nature (London) **498**, 470 (2013).
[49] R. Terawaki, Y. Takahashi, M. Chihara, Y. Inui, and S. Noda, Opt. Express **20**, 22743 (2012).
[50] Y. Takahashi, H. Hagino, Y. Tanaka, T. Asano, and S. Noda, Opt. Express **15**, 17206 (2007).
[51] T. Asano, Y. Ochi, Y. Takahashi, K. Kishimoto, and S. Noda, Opt. Express **25**, 1769 (2017).
[52] D. F. Edwards, *Handbook of Optical Constants of Solids* (Academic, New York, 1997), Vol. I, Part II, pp. 547–569.
[53] G. Davies, Phys. Rep. **176**, 83 (1989).
[54] K. Nozaki, S. Kita, and T. Baba, Opt. Express **15**, 7506 (2007).
[55] T. Uesugi, B.-S. Song, T. Asano, and S. Noda, Opt. Express **14**, 377 (2006).
[56] J. Upham, Y. Tanaka, Y. Kawamoto, Y. Sato, T. Nakamura, B.-S. Song, T. Asano, and S. Noda, Opt. Express **19**, 23377 (2011).